1

Mechanical Properties of Amorphous Silicon Carbide

Kun Xue[1], Li-Sha Niu[2] and Hui-Ji Shi[2]
[1]*State Key Laboratory of Explosion Science and Technology, Beijing Institute of Technology*
[2]*School of Aerospace, FML, Department of Engineering Mechanics, Tsinghua University, Beijing, China*

1. Introduction

Excellent physical and chemical properties make silicon carbide (SiC) a prominent candidate for a variety of applications, including high-temperature, high-power, and high-frequency and optoelectronic devices, structural component in fusion reactors, cladding material for gas-cooled fission reactors, and an inert matrix for the transmutation of Pu(Katoh, Y. et al., 2007; Snead, L. L. et al., 2007). Different poly-types of SiC such as 3C, 6H of which 6H have been researched the most. There has been a considerable interest in fabricating 3C-SiC/6H-SiC hetero p-n junction devices in recent years. Ion implantation is a critical technique to selectively introduce dopants for production of Si-based devices, since conventional methods, such as thermal diffusion of dopants, require extremely high temperatures for application to SiC. There is, however, a great challenge with ion implantation because it inevitably produces defects and lattice disorder, which not only deteriorate the transport properties of electrons and holes, but also inhibit electrical activation of the implanted dopants(Benyagoub, A., 2008; Bolse, W., 1999; Jiang, W. et al., 2009; Katoh, Y. et al., 2006). Meanwhile the swelling and mechanical properties of SiC subjected to desplacive neutron irradiation are of importance in nuclear applications. In such irradiations the most dramatic material and microstructural changes occur during irradiation at low temperatures. Specifically, at temperatures under 100˚C volumetric swelling due to point defect induced strain has been seen to reach 3% for neutron irradiation doses of ~0.1-0.5. At these low temperatures, amorphization of the SiC is also possible, which would lead to a substantial volumetric expansion of ~15%, along with decreases in mechanical properties such as hardness and modulus(Snead, L. L. et al., 1992; Snead, L. L. et al., 1998; Snead, L. L., 2004; Weber, W. J. et al., 1998).

Intensive experimental and theoretical efforts have been devoted to the dose and temperature dependence of the properties of irradiation-amorphized SiC (a-SiC)(Weber, W. J. et al., 1997). Heera *et al*. (Heera, V. et al., 1997) found that the amorphization of SiC induced by 2 MeV Si^+ implantation is accompanied by a dramatic and homogeneous volume swelling until a critical dose level dependent on the temperature. Afterwards the volume tends to saturate and the density of *a*-SiC is about 12% less than that of the crystalline

material. The experimental values of the elastic modulus and hardness of a-SiC estimated from measurements of surface and buried amorphous layers show a large degree of variability. In general, the hardness and elastic modulus in *a*-SiC are observed to decrease 20%-60% and 25%-40%, respectively. Weber *et al.*(Weber, W. J. et al., 1998) performed nanoindentation experiments with Berkovich indenter on the Ar^+ beam induced *a*-SiC. The results suggest that the elastic modulus decreases ~24%, from 550 to 418 GPa. Snead *et al.*(Snead, L. L. et al., 1992) reported that the elastic modulus in SiC, irradiated with C^+ at low temperatures, decrease from 400 GPa in the virgin region to about 275 GPa in the amorphized region; whereas the hardness was observed to decrease from 41 to 32 GPa. The mechanical properties of a-SiC irradiated by neutron have also been investigated(Snead, L. L. et al., 1998). A density decrease of 10.8% from the crystalline to amorphous (c-a) state is revealed along with a decrease in hardness from 38.7 to 21.0 GPa and a decrease in elastic modulus from 528 to 292 GPa.

The varying amorphous nature of a-SiC depending on the damage accumulation could justify the wide range of experimental measurements of mechanical properties of a-SiC. Thus of particular fundamental and technological interest has been developing the models capable of describing the various physical properties of SiC as a function of microstructural changes, specifically from c-a. Gao and Weber(Gao, F. & Weber, W. J., 2004) investigated the changes in elastic constants, the bulk and elastic moduli of SiC as a function of damage accumulation due to cascade overlap using molecular dynamics (MD) simulation. The results indicate a rapid decrease of these properties with increasing dose but the changes begin to saturate at doses greater than 0.1 MD-dpa. Given that fully amorphous state is reached at a dose of about 0.28 MD-dpa, they suggested that point defects and small cluster may contribute more significantly to the changes of elastic constants than the topological disorder associated with amorphization.

Although the inherent correlation between the mechanical properties and the disordered microstructures of *a*-SiC has been widely accepted, there still lacks a comprehensive description of this correlation given the intricate nature of a-SiC. Thus based on detailed examinations of an extensive series of simulated *a*-SiC models with varying concentration of defects, this chapter first attempts to characterize the structure of *a*-SiC with a range of underpinning parameters, whereby substantiates the correlation between the amorphous structure of SiC and a variety of mechanical properties. MD simulations are used to simulate the mechanical responses of varied disordered SiC microstructures subject to two typical loadings, namely axial tension and nanoindentaion, which are critical for measures of strength and ductility of bulk *a*-SiC and hardness of *a*-SiC film. The role of these simulations is not necessarily to reproduce exact experimental behaviors, but rather to identify possible atomistic mechanisms associated with a variety of disordered SiC structures, especially from c-a.

Amorphous materials often exhibit unique deformation mechanisms distinct from their crystalline counterparts. The coexistence of brittle grains and soft amorphous grain boundaries (GBs) consisting in nanocrystalline SiC (nc-SiC) results in unusual deformation mechanisms. In the simulation of nanoindentation(Szlufarska, I. et al., 2005), as the indenter depth increases, the deformation dominated by the crystallization of disordered GBs which "screen" the crystalline grains from deformation switches to the deformation dominated by disordering of crystalline grains. Plastic flow along grain boundaries can also effectively

suppresses the cavity nucleation, leading to increased ductility and toughness without compromising its strength(Mo, Y. & Szlufarska, I., 2007).

Because amorphous materials lack a topologically ordered network, analysis of deformations and defects presents a formidable challenge. Conventional computational techniques used for crystalline solids, such as the modulus of slip vector(Rodriuez de la Fuente, O. et al., 2002), centrosymmetry, and local crystalline order, fail to identify the deformation defects in disordered materials. Various models have been proposed to describe defects in such structures. The prevailing theory of plasticity in metallic glasses involves localized flow events in shear transformation zones (STZ)(Shi, Y. & Falk, M. L., 2005). An STZ is a small cluster of atoms that can rearranges under applied stress to produce a unit of plastic deformation. It is worth noting that most of these theories are based on the observations of metallic glasses. Whereas covalently bonded amorphous solids differs from their metallic counterparts due to their directed stereochemical bonds in forms of well-defined coordination polyhedral, e.g. [SiX4]or [CX4] tetrahedra in SiC. Thanks to the short range order retained in the amorphous covalent materials, plastic deformation tends to be more pronounced localized than in the case of metallic glasses(Szlufarska, I. et al., 2007). Moreover for amorphous alloys like *a*-SiC, the degree of chemical order has been always under the debates, although the consensus from these recent experimental studies of *a*-SiC seems to be in favor of the existence of C-C homonuclear bonds(Bolse, W., 1998; Ishimaru, M. et al., 2002; Ishimaru, M. et al., 2006; Snead, L. L. & Zinkle, S. J., 2002). The presence of dual disorder, namely chemical and topological disorder, in *a*-SiC definitely complicates the analysis of amorphous structure and the underlying atomic mechanisms.

In general a truly atomistic model of plastic flow in amorphous covalent materials is still lacking. Instead of starting with complete *a*-SiC where widespread inhomogenities frozen into the entire material, we rather begin with a perfect 3C-SiC, then proceed to gradually increase the concentration of damage until a complete amorphous state is reached. Being a link between perfect crystalline and complete amorphous SiC, partially disordered SiC presents a favorable prototype to discern the role of isolated or clustered defects in the evolution of atomic mechanism, where the deformation defects are comparatively readily to identify.

In this chapter, we first outline the studies concerning the c-a transition of irradiation-amorphized SiC, laying the basis for the analysis of SiC amorphous. Then a complete topological description of simulated SiC structures ranging from c-a is presented in both the short – and medium-range with a special focus on the correlation between chemical disorder and the topology of *a*-SiC. Simulated tensile testing and nanoindentation are carried out on the varying *a*-SiC to examine the variations of mechanical response with varying concentration of defects. The correlation between some key mechanical properties of *a*-SiC, such as Young's modulus, strength, hardness, and the microstructure are quantified by virtue of chemical disorder, an characteristics underpinning the c-a transition. A crossover of atomic mechanisms from c-a are also discussed. This crossover is also embodied in the switch of the fracture .

2. Amorphization mechanism of irradiation-amorphized SiC

With regard to the characterization of the varying disordered microstructures of *a*-SiC, the mechanisms controlling the c-a transformation have been of particular interest. By simulating the accumulation of irradiation damages due to the low energy recoils, Malerba

and Perlado(Malerba, L. & Perlado, J. M., 2001) argued that both Frenkel pairs and antisite defects play significant roles in the amorphization process and that the coalescence and growth of defect clusters account for the amorphization of SiC. Antisite defects were found to be less numerous than Frenkel defects, whose accumulation has been instead primarily supposed to trigger amorphization. However Frenkel pairs have strong correlation with antisites. The MD simulation of the disordering and amorphization processes in SiC irradiated with Si and Au ions reveals much higher concentration of antisites in complete amorphous areas where are supposed to comprise large amount of Frenkel pairs than other disordered domains(Gao, F. & Weber, W. J., 2001). Furthermore where is significant overlap of antisite coordination shells, where there are a significant number of Frenkel pairs that are accommodated. If completely excluding antisites, Frenkel defects would become extremely unstable, leading to difficulties of amorphization. Rong *et al*.(Rong, Z. et al., 2007) simulated the recovery of point defects created by a single cascade during the thermo annealing via dynamic lattice MD technique. The results suggest that a large number of irradiation induced Frenkel pairs are formed in metastable configurations, and majority of close pairs would recombine during the annealing at 200 K and 300 K. Contrasting with the dramatic annihilation of Frenkel defects upon annealing, the number of antisite largely remains constant even increases somewhat due to the recombination of interstitials from one sublattice with vacancies on the other. Therefore the role of antisite in the amorphization of SiC is of equal essence.

Basically both Frenkel and antisite defects could give rise to dual disorder, namely topological and chemical disorder. Homonuclear bonds (C-C, Si-Si) are likely to form when antisite or Frenkel defects are introduced, producing a certain degree of chemical disorder. The homonuclear bond ratio R_{hnb}, defined for SiC as the ratio of number of homonuclear bonds to twice the number of heteronuclear bonds, provides a full homonuclear bond analysis. Chemical disorder χ(Tersoff, J., 1994), defined as the ratio of C-C bonds to C-Si bonds, $N_{\mathrm{C\text{-}C}}/N_{\mathrm{Si\text{-}C}}$, is not a full homonuclear bond analysis and is specified only for C atoms. The argument for using χ instead of R_{hnb} derives mostly from the practical uncertainty of enumerating Si-Si bonds in amorphous structures for which Si atoms have no clearly defined first coordination shell. In practice, χ is quite a good approximation to R_{hnb} and the deviation is proportional to the coordination number difference between Si and C.

The topological disorder of *a*-SiC manifests itself in variations of the short- and medium-range. Short-range order (SRO), as its name implies, concerns structural order involving nearest-neighbour coordination shell. This is easiest to discuss in the case of covalently bonded amorphous solids since the presence of their directed stereochemical bonds simplifies the description considerably. For example, in the case of SiC, SRD is defined in terms of well defined local coordination tetrahedra. The parameters which are sufficient to describe topological SRO in stereochemical systems are the (coordination) number, N_{ij}, of nearest neighbors of type j around an origin atom of type i, the nearest-neighbour bond length R_{ij}, the bond angle subtended at atom i, θ_{jik} (when the atom of type k is different from j). The connectivity of polyhedral dictates the type and extent of medium-range order (MRO). Shortest-path ring(Rino, J. P. et al., 2004), defined as a shortest path consisting of nearest-neighboring atoms, and local cluster primitive ring(Yuan, X. & Hobbs, L. W., 2002) are among often used means to characterize the MRO. Because Frenkel pairs and anitisites have overlapping effects on the amorphization of SiC, and exclusively focusing on the formal Frenkel pairs and antisite configuration themselves has ignored the multiplier effects

on the immediate coordination of a much larger number of atoms, hierarchical parameters signifying SRO and MRO seem to be more appropriate to describe the c-a transition and varying microstructures of *a*-SiC. The c-a transition is accordingly described in terms of the variations in the chemical disorder χ and other topological parameters. The correlation between them would be clarified in the next section.

3. Characterization of the structures of *a*-SiC

Considerable investigations, including experimental and MD simulation studies, indicate a strong correlation between chemical and topological disorder. The x-ray absorption and Ramann spectroscropy performed by Bolse(Bolse, W., 1998) on Na^+ irradiated SiC clearly showed that a large fraction of the [SiC_4] tetrahedra is destroyed only after the removal of chemical order. The inspection of MD simulated melt-quenched *a*-SiC Has also revealed that chemical disorder determines the short- and medium-range topological order in *a*-SiC(Xue, K. et al., 2008). Therein an extended tetrahedron model only dependent on the composition and chemical disorder χ was developed to predict the probabilities of various local coordination tetrahedra, namely, Si-$Si_{4-n}C_n$ and C-$Si_{4-n}C_n$ (n = 0-4), reflecting the local spatial distribution of homonuclear bonds.

(χ)	C4	Si4	$l_{C\text{-}C}$	$l_{Si\text{-}C}$	$l_{Si\text{-}Si}$	Density ($\times 10^3$ Kg/m^3)	Potential Energy (eV/atom)
0.0	100.	100.	N	1.896	N	3.217	-6.39279
0.045	99.9	99.6	1.662	1.862	2.185	3.213	-6.32738
0.133	99.5	98.9	1.661	1.867	2.191	3.148	-6.21825
0.24	98.4	97.8	1.648	1.872	2.225	3.087	-6.10155
0.39	96.1	95.1	1.646	1.877	2.258	3.063	-5.99751
0.422	96.3	92.1	1.635	1.880	2.28	3.058	-5.9726
0.54	96.2	84.1	1.610	1.885	2.337	3.053	-5.88191
0.7	94.2	83.5	1.585	1.904	2.379	3.049	-5.81427

Table 1. Structural characteristics and potential energies of chemical disordered SiC with varying χ. Notations: X4 (X = C or Si), the percentage of four-fold coordinated X atoms; $l_{X\text{-}Y}$ (X, Y = C or Si), the average bond length of X-Y bond. In our calculations the cut-off distances of the C-C, Si-C, and C-C interactions are 1.75 Å, 2.0 Å and 2.5 Å, respectively.

The inspection of MD simulated irradiation-induced *a*-SiC has investigated the changes of topological order as a function of chemical disorder and suggested that some threshold chemical disorder should be one requirement for amorphization(Xue, K. & Niu, L.-S., 2009; Yuan, X. & Hobbs, L. W., 2002). Herein interatomic interactions were modeled using the 1994 Tersoff potential improved by Tang and Yip(Tang, M. & Yip, S., 1995; Tersoff, J., 1994). Devanathan et al.(Devanathan, R. et al., 2007) compared the structures of modeled melt-quenched *a*-SiC obtained from three different potentials, namely Tersoff, Brenner, and ionic potentials, with the results of a tight-binding MD (TBMD) simulation and an *ab initio* study. They found that the structural features of *a*-SiC given by Tersoff potential appear to be in better agreement with *ab initio* and TBMD results. In order to explore the role of chemical disorder in the changes of SiC topology, varying chemical disorder ranging from 0 to 0.7 are imposed on a set of 3C-SiC perfect crystal models by swapping pairs of random sites.

The SRO and MRO of all SiC assemblies with varying imposed chemical disorder are examined in terms of a variety of parameters, such as coordination number, pair correlation functions $g_{\alpha\beta}$(r) and local cluster primitive ring statistics. Table 1 summaries the variations of some important SRO indicators of *a*-SiC with varying χ. The number of four-fold coordinated C and Si atoms declines with increasing χ especially for the case of Si atom, which is in accordance with the argument in Sec. 2 that more interstitials (vacancies) are accommodated in the areas abundant in antisites. Another feature worth noting is the significant lengthening of C-C bond and the shortening of Si-Si and Si-C bonds, the trend being more pronounced for small χ.

The two body structural correlations of the amorphous materials are analyzed by pair correlations functions $g_{\alpha\beta}(r)$. The evolution of MRO can be traced in terms of the local cluster primitive (LC) ring content, defined as a closed circuit passing through a given atom of the network which cannot be decomposed into two smaller circuits. The LCs haven been shown to uniquely characterize the topologies of all compact crystalline silica, Si_3N_4 and SiC polymorphs(Hobbs, L. W. et al., 1999). In the case of crystalline *a*- or β-SiC, the LCs comprises 12 6-rings (as in Si).

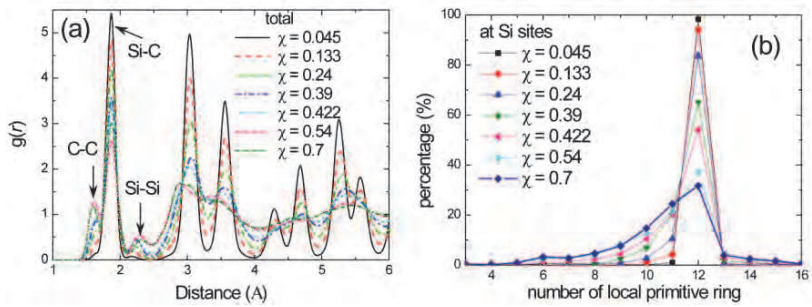

Fig. 1. (a) Total pair correlation function $g_{\alpha\beta}(r)$ and (b) distribution of local cluster ring number at Si sites for *a*-SiC samples with varying chemical disorder(Xue, K. & Niu, L.-S., 2009).

Fig. 1(a) shows the $g_{\alpha\beta}(r)$ for the SiC assemblies with increasing χ. The C-Si peak substantially declines as χ increases accompanying the enhancement of the C-C and Si-Si peaks. Any appreciable changes of $g_{\alpha\beta}(r)$ could barely be identified after $\chi \sim 0.5$, in a sense meaning the saturation of short-range disordering. Fig. 1(b) demonstrates that the majority of the LCs for $\chi < 0.24$ consist of 12 6-SiC as in 3C-SiC, significant changes of LCs contents occur within the range of $0.24 < \chi < 0.54$, and afterwards the changes tend to saturate. The chemical disorder dependences of SRO and MRO depict the same picture: perfect topological order in 3C-SiC structure is energetically stable until chemical disorder reaches beyond the $\chi = 0.24 - 0.42$ range; for $\chi \geq 0.54$, topological perfection appears impossible to maintain and a stable amorphous structure is achieved.

4. Tensile testing simulation of *a*-SiC

4.1 Variations in elastic properties of SiC from crystalline to amorphous

Gao and Weber(Gao, F. & Weber, W. J., 2004) calculated the changes of elastic constants, C_{11}, C_{12}, C_{44}, the bulk modulus, B, and averaged elastic modulus, E as a function of dose for cascade-amorphized SiC by imposing moderate strain (<1%) along the MD cell axes. All

elastic constants and elastic modulus show expected softening behavior under irradiation for the dose range of interest. Fig. 2 shows their typical results with regard to the variations of elastic modulus, E and bulk modulus B. These elastic properties decrease rapidly at doses less than 0.1 MD-dpa, and the decrease becomes smaller at the high dose levels. On account of the dose dependence of the formation and coalescence of point defects and small clusters, they concluded that point defects and small clusters contribute much greater than topological disorder to the degradation of elastic properties of *a*-SiC.

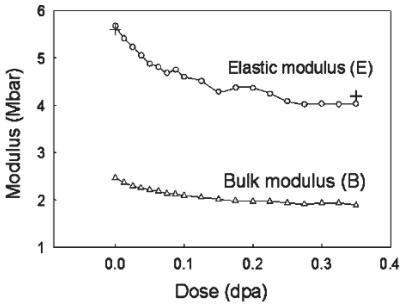

Fig. 2. variation of elastic modulus, *E*, and bulk modulus, *B*, as a function of dose(Rino, J. P. et al., 2004)

4.2 Tensile mechanical response of *a*-SiC

Point defects, small clusters and topological disorder as forms of defect accumulation could somehow indicate the dependence of mechanical properties of *a*-SiC on the disordered microstructure. However it is difficult to enumerate these damages due to the ambiguous definitions of their complicated configurations. Bearing in mind that chemical disorder χ is of essence to trigger the c-a transition as elucidated in Sec.3, chemical disorder χ is able to distinguish varying disordered SiC structures. Thus formulating the correlation between a variety of mechanical properties and chemical disorder χ provide a favorable alternative to quantify the microstructure dependence of mechanical properties.

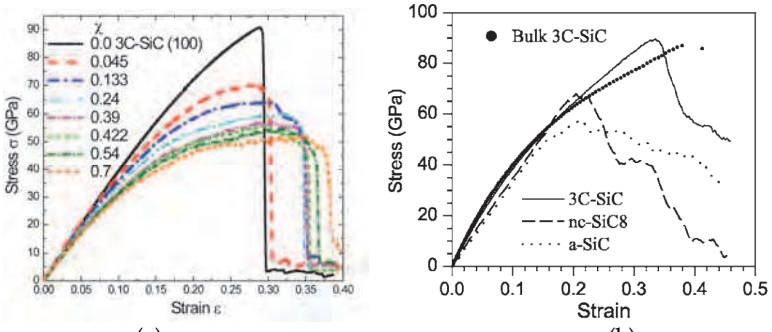

(a) (b)

Fig. 3. (a) stress vs strain curves for *a*-SiC samples with varying chemical disorder at a strain rate of $10^8 s^{-1}$ (Xue, K. & Niu, L.-S., 2009); (b) stress vs strain curves for 3C-SiC, nc-SiC and melt-quenched *a*-SiC with an extension rate of 100 m/s(Ivashchenko, V. I. et al., 2007)

Simulated axial tensile testing is carried out on a set of SiC assemblies with varying chemical disorder χ, representing a range of disordered structures from crystalline to complete amorphous. The full stress-strain dependences for different SiC assemblies with varying χ are shown in Fig. 3. The stress-strain curve for 3C-SiC features a linear elastic stage ending up with an abrupt drop of the stress, while the presence of negligible chemical disorder χ (χ=0.045) gives rise to a noticeable deviation beyond $\varepsilon \approx 0.13$ from what would be expected from extrapolation of the linear elastic region. Meanwhile an appreciable softening of the material after the stress reaches σ_{max} can be observed, evidenced by the weak decrease of the stress before the rupture. This plasticlike behavior becomes increasingly evident with increasing χ, pronounced plastic flow plateau covering a major part of the whole mechanical response. Such plasticelike behavior is reproduced in the tension of simulated melt-quenched *a*-SiC with a drastic reduction in the number of tetrahedrally coordinated atoms(Ivashchenko, V. I. et al., 2007).

4.3 Mechanical properties of *a*-SiC as a function of chemical disorder χ

The chemical disorder dependence of the mechanical response of *a*-SiC is likewise embodied in the variations of the Young's modulus and strength of *a*-SiC with varying chemical disorder [Fig. 4]. Young's modulus and strength generally exhibit monotonic decrease with increasing χ while in distinct manners until χ reaches 0.54, afterwards tend to saturate regardless of the further increase of χ. Young's modulus E_Y shows negative linear dependence on χ within the range of $0 < \chi < 0.54$ as follows:

$$E_Y = 0.9994E_{Y_0} - 0.316 \times \chi \times E_{Y_0} \quad (1)$$

where E_{Y0} is Young's modulus along the [100] direction of 3C-SiC (~413 GPa). Young's modulus of complete *a*-SiC is around ~321.4 GPa, agreeing well with the value calculated for the melt-quenched *a*-SiC which stands at ~327 GPa(Ivashchenko, V. I. et al., 2007). In contrast with the consistent reduction of E_Y with increasing χ before $\chi < 0.54$, a dramatic decrease of 23.2% for strength occurs at $\chi = 0.045$, decreasing from ~90.8 GPa ($\chi = 0$) to ~69.7 GPa ($\chi = 0.045$). Whereas strength almost linearly declines afterwards with increasing χ as the following relation until χ =0.54,

$$S = 0.745S_0 - 0.328 \times \chi \times S_0 \quad (2)$$

where S_0 is the strength of 3C-SiC (~90.8 GPa). When χ is beyond 0.54, a complete amorphous state is reached, Young's modulus and strength tend to be constant, which is in line with the saturation of Elastic moduli of *a*-SiC at high doses(Gao, F. & Weber, W. J., 2004).

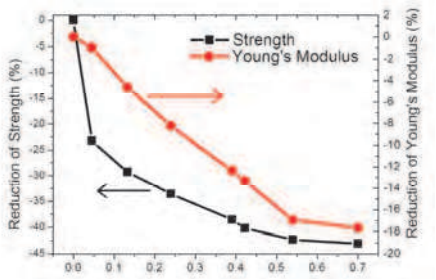

Fig. 4. Variations of Young's modulus and strength as a function of chemical disorder(Xue, K. & Niu, L.-S., 2009)

4.4 Deformation mechanims

In order to gain further insights into the chemical disorder dependece of Young's modulus and strength, the knowledge of the deformation mechanims of varying disordered structures is necessary. Young's modulus of the covalent network is closely related with the ability of the topological network to homogeneously elastic deform to accomadate the small strain. Despite of the presence of moderate chemical disorder χ, the almost intact conection of fundamental tetrahedral units, as well as their relative orientation, ensure the homogeneously collective deformation of these units at small χ. Thus no appreciable decrease of Young's modulus could be detected for the SiC assembly with χ = 0.045. As χ increases, the topological order gradually decays, resulting in the reduced stiffness of the network and The ensuing decrease of Young's modulus until a complete amorphous state is reached. Actually the linear elastic region of mechanical response of *a*-SiC gradually diminishes with the increasing χ.

Although a handfull of homonuclear bonds introduced by a negligeable chemcial disorder (χ = 0.045) barely affect the topological order and the Young's modulus, they account for a substantial decline of strength. Due to the atom size difference, the C-C bonds in the undeformed system have been stretched with a bond length increase of ~7% contrasting to the contraction of Si-C and Si-Si bonds. With the strain processes, these stretched C-C bonds are expected to break prior Si-C and Si-Si bonds. The premature breakage of C-C bonds disconnects the neighboring tetrahedral network where the stress builds up. More decohesions of atomic bonds therein conversely take place due to the localized stress. As a results, Localized softened clusters around the initial chemical disorderd sites are formed, where atomic rearrangements dominate the confined plastic flow. Fig. 5 (a) illustrates the atomic slipping occurring in these softened regions. With the inceased χ, the enhanced topological disorder gives rise to the prevalence of softening regions. Thus the localized plastic flow evolves into percolating flow through the entire system [Fig. 5(b)].

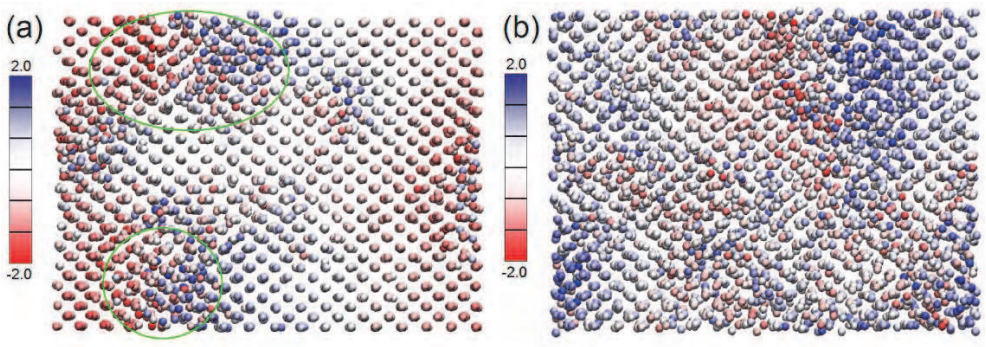

Fig. 5. Atomic configurations for (a) the χ = 0.045 and (b) the χ = 0.39 assemblies at ε = 0.27. Atoms are colored according to their motion relative to the homogeneous deformation. Blue atoms have moved towards right relative to what would be expected if the deformation had been homogeneous and elastic; red atoms have moved towards left. The scale indicates how the atoms have moved (in angstroms)(Xue, K. & Niu, L.-S., 2009).

4.5 Fracture modes

When the disorder SiC undergoes c-a transition with the increasing chemical disorder χ, the main deformation mechanism evolves from elastic deformation to localized atomic rearrangement, and then to percolating plastic flow. This crossover is also manifested itself in the switch of the fracture mechanism. At a slight chemical disorder (χ =0.045), localized softened clusters are embedded in the rigid topological ordered lattice which strongly supresses the nucleation of nanocavities inside the disordered clusters. Thus the failure of ligaments between softened clusters rather than the percolation of nanocavities leads to the final brittle fracture, which is supported by the sudden drop of cavity density at ε ~0.3 [Fig.6]. Increased chemical disorder substantially alters the atomistic picture of fracture mechanisms. In the fully amorphous system (χ = 0.54), extensive plastic flow nucleates a large number of nanocavites, their coalescence and percolation through the system leading to the final fracture. This argument is consistent with the slow decline of cavity desity after ε ~0.23 for the χ = 0.54 assembly [Fig. 6]. For *a*-SiC with moderate chemical disorder (0 < χ < 0.54), we can expect a competition of brittle and ductile fracture mechanism, dominated by lattice instability and coalescence of nanocavities, respectively.

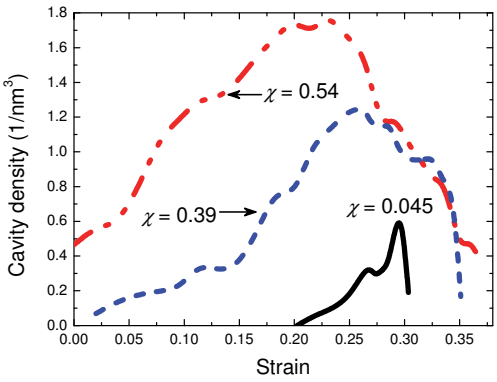

Fig. 6. Cavity densities as a function of strain (a) for different *a*-SiC samples with varying chemical disorder at a strain rate of 10^8 s^{-1} and (b) for the χ = 0.54 ensemble at different strain rates(Xue, K. & Niu, L.-S., 2009).

Recently special efforts have been made to reveal the possible crossover of fracture modes during c-a transition. Glassy materials are considered up to now as the archetype of pure brittle materials, the brittle fracture of which proceeds solely by decohesion of atomic bonds at the crack tip. However, AFM and high scanning electron microscopy (SEM) studies have generated considerable controversy about the nature of fracture mechanism in brittle amorphous solids(Celarie, F. et al., 2003). Xi *et al.*(Xi, X. K. et al., 2005) found a dimple structure at the fracture surface of Mg-based bulk metallic glass by high resolution SEM, indicating that the fracture in brittle metallic glassy materials might also proceed through the softening mechanism but at nanometer scale. Chen *et al.*(Chen, Y.-C. et al., 2007) further investigates the interaction of voids in silica glass by means of multimillion-to-billion-atom MD simulation, unveiling the mechanism of nanocavities nucleation. These findings are in line with the ductile fracture observed in *a*-SiC with $\chi \geq 0.54$ mediated by coalescence of cavities similar to metal materials, although taking place at different length scales.

5. Nanoindentation simulations of *a*-SiC

5.1 P-h curves of *a*-SiC

Nanoindentation is a widely used technique for probing mechanical properties and stability, especially of surfaces and thin films. From the shape of load-indenter displacement (*P-h*) curves, one can extract information about elastic moduli or hardness. Atomistic computer simulations have been found very helpful in unraveling the processes underlying the nanoindentation responses. For example, MD simulations of indentation of 3C-SiC have shown that the *p-h* curve [Fig.7(b)] is correlated with the nucleation and coalescence of dislocations under an indenter(Szlufarska, I. et al., 2005).

Amorphous materials lack a long-range order of topological network and hence there is no clear notion of dislocations. Thus understanding atomistic processes during nanoindentation in amorphous materials presents a great challenge. A few atomistic simulations have been performed to tackle this problem. Szlufarska *et al*.(Szlufarska, I. et al., 2007) undertook the difficult task of simulating nanoindentation of melt-quenched *a*-SiC with a diamond indenter. The simulation reveals a noticeable localization of damage in the vicinity of the indenter, however the localization is less pronounced than in the case of 3C-SiC. As shown in Fig. 7(a), the *P-h* curve for *a*-SiC exhibits irregular, discrete load drops similar to 3C-SiC [Fig. 7(b)]. Here, the load drops correspond to braking of the local arrangements of atoms, in analogy to the slipping of atomic layers in 3C-SiC. Simulations also show that, even at indentation depth *h* smaller than those at which the material yields plastically, the material's response is not entirely elastic. Instead, the amorphous structure, which is metastable by nature, supports a small inelastic flow related to relaxation of atoms through short migration distances.

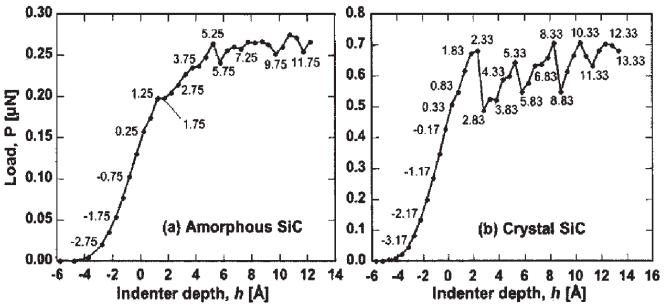

Fig. 7. Load-displacement (*P-h*) responses for (a) *a*-SiC and (b) 3C-SiC(Szlufarska, I. et al., 2007)

As aforementioned imposing increasing chemical disorder χ on 3C-SiC is able to produce a series of disordered SiC structures ranging from perfect crystalline to complete amorphous, providing favorable prototypes to observe the dependence of hardness on the damage accumulation. More importantly, this means could allow us to identify possible atomistic mechanisms in the early stages of plastic deformation as a function of microstructure. A set of disordered SiC assemblies with varying chemical disorder χ are established as the substrates in the means introduced in Sec.2. The Geometrical setup of the indenter and the substrate is detailed in ref(Xue, K. & Niu, L.-S., 2010). In the case of 3C-SiC, the x, y, z directions correspond to the $[\bar{1}10]$, $[001]$ and $[110]$ crystallographic directions, respectively.

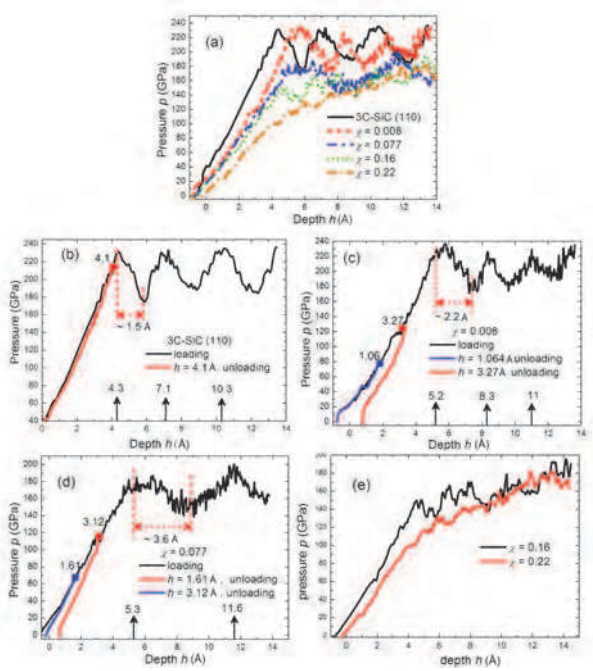

Fig. 8. Pressure-depth (*p*-*h*) response: (a) comparison of loading curves for 3C-SiC and *a*-SiC with varying chemical disorder. (b) Loading and unloading curves from h = 4.1 Å (red) for 3C-SiC. (c) Loading and unloading curves from h = 1.06 Å (blue) and h = 3.27 Å (red) for the χ = 0.008 assembly. (d) Loading and unloading curves from h = 1.61 Å (blue) and h = 3.12 Å (red) for the χ = 0.077 assembly. (e) Loading curves for the χ = 0.16 and the χ = 0.22 assemblies(Xue, K. & Niu, L.-S., 2010).

Fig.8 shows the computed *p*-*h* curves for varying SiC assemblies. Here the pressure (p) defined as the load P divided by actual contact is plotted as a function of depth h. For (110) surface of 3C-SiC, *p*-*h* curve displays a linear elastic region followed by a series of sudden load drops occurring at depths equally spaced by ~3 Å, resembling the simulated *P*-*h* curve of 3C-SiC modeled using an interatomic potential developed by Vashishta *et al*.(Szlufarska, I. et al., 2005). The *p*-*h* curves of the χ = 0.008 assembly is similar to the case of 3C-SiC featuring roughly equally spaced peaks after the yield. Whereas the position of the first peak at which the maximum pressure is achieved is significantly deferred accompanying noticeable broadening of peaks. The alteration becomes increasingly pronounced with increasing χ. For the χ = 0.077 assembly, pressure peaks enveloping numerous small serrations are considerably broadened with a much larger separation of ~6 Å. Meanwhile the intensity (peak pressure) and magnitude (the amount of load drop) of peaks are substantially reduced. Given that the disordered atoms just account for ~3.5% and ~5% of total atoms for the χ = 0.008 and χ = 0.077 assembly, respectively, the changes of the *p*-*h* response seem striking. The defined peak structures of the *p*-*h* curves evolves into irregularly spaced fluctuations for the χ = 0.16 assembly and small oscillations in the χ = 0.22 assembly. These substantial changes of the *p*-*h* response with increasing χ suggest a crossover of underlying atomistic mechanisms, as we will discuss later.

5.2 Hardness

The hardness (H) is usually defined as equal to the peak force applied during indentation divided by the projected contact area. The calculated values of hardness here are estimated by yield strength. For 3C-SiC and *a*-SiC with low or moderate chemical disorder ($\chi \leq 0.16$), yield strength is taken as the pressure of the first peak maximum signifying the onset of structural instability. However, the monotonically ascent *p-h* curve for the χ = 0.22 assembly displays a kink rather than distinguishable load peaks, so the pressure at the kink is picked up as the measure of calculated hardness. It's worth noting that the contact pressure deprived from nanoindentation simulations is usually several times greater than the experimental hardness(Mulliah, D. et al., 2006; Noreyan, A. et al., 2005). One major reason is the fact that the indenter size used in the MD simulations is always smaller by two or three orders of magnitude than the indenter used in experiments. According to a relation between contact pressure (p) and the indenter size at the onset of the nucleation of dislocation(Liu, X. M., 2008), we can readily convert the calculated yield strength into the equivalent hardness.

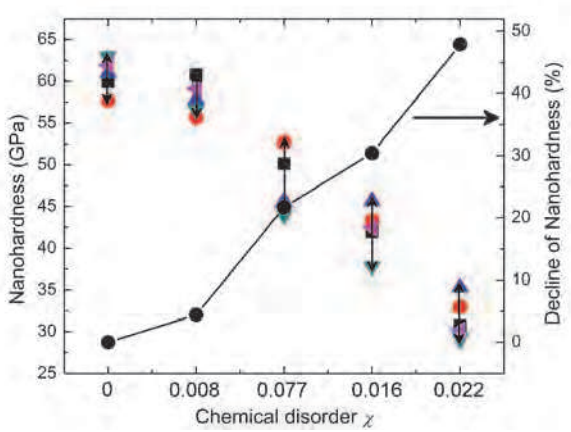

Fig. 9. Calculated hardness of disordered SiC with increasing chemical disorder(Xue, K. & Niu, L.-S., 2010)

The calculated hardness values for different SiC assemblies are plotted in Fig. 9. A remarkable reduction of hardness can be observed for the χ = 0.077 assembly. For the complete *a*-SiC assembly with χ = 0.22, the hardness value is ~50% less than in 3C-SiC which agrees with the reduction of hardness in *a*-SiC observed in the experiments(Khakani, M. A. E. & al, e., 1994).

5.3 Atomistic mechanisms

The distinctive characteristics of the *p-h* curves of SiC from c-a could be understood in light of the corresponding atomistic mechanisms, which entail the detailed analysis of the evolution of the associated microstructures with the increasing indent depth h. The shortest path ring distribution has been widely used to identify the subsurface defects during the nanoindentation(Szlufarska, I. et al., 2004). The presence of nonthreefold rings marks the occurrence of structural deformation, most likely the presence of dislocations.

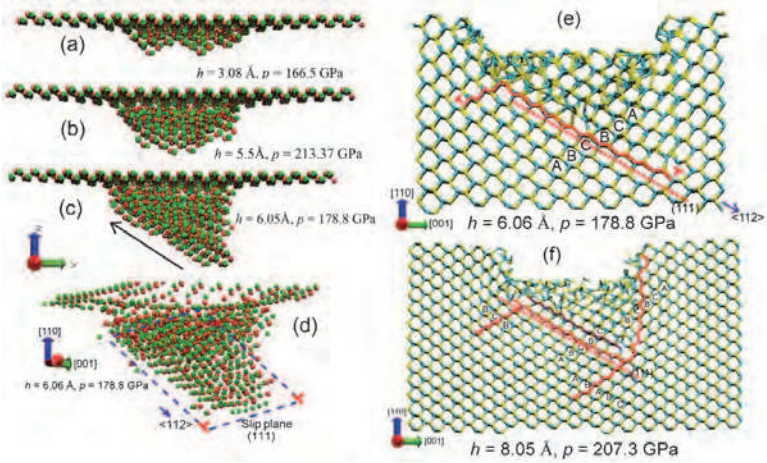

Fig. 10. $(\bar{1}10)$ projections of indentation damages in 3C-SiC composed by disordered atoms with non-threefold rings at different depths. (a) h = 3.08 Å, (b) h = 5.5 Å, (c) h = 6.05 Å. (d) shows the (111) slip plane along which the slip of atomic layers occur at h = 6.05 Å. (e) and (f) illustrate the $(\bar{1}10)$ projections of 3C-SiC structure beneath the indenter after the first slip and the second slip of atomic layers, respectively. A stack fault along the red line (e) exists in (111) plane, which is terminated with a Shockley partial dislocation along the [110] direction with Burgers vector 1/6[112]. A second outburst of dislocations occurs on next (111) plane just below the first (111) plane (f).(Xue, K. & Niu, L.-S., 2010)

The atomistic mechanisms of 3C-SiC during indentations have been elaborated in quite a few of publications(Chen, H.-P. et al., 2007; Szlufarska, I. et al., 2004, 2005; Xue, K. & Niu, L.-S., 2010). Herein some basic deformation mechanisms related to the nanoindentation of 3C-SiC (110) surface with the cuboidal indenter are to be laid out in order to how the atomistic deformation determines the mechanical response, namely *p-h* curves. Basically the series of equally spaced sudden load drops can be attributed to the dissipation of accumulated stress by subsequent breaking of atomic layers of the substrate whose separation in the indentation (z) direction (here that is [110] crystallographic direction). Fig. 10 (a)-(d) demonstrates the atomic configurations which contain only nonthreefold rings before and after the onset of plastic yield. Fig. 10 (b) and (c) clearly shows the bending and slipping in (111) plane of sequent atomic layers under the indenter, corresponding to the accumulation and release of the load, respectively. The first dislocation emits from the corners of the indenter after the slip and resides in the (111) plane [Fig.10 (e)]. The following dislocation arising from the second slip of atomic layers initiates on the next below (111) plane [Fig. 10(f)]. Two stack faults existing on the neighboring {111} planes can be identified after the second load drop [Fig.01(f)], forming a thin layer of hexagonal (wurtzite) structure in the face-centered cubic (zinc-blende) structure of crystalline grains. Similar type of defect has been observed in the indentation of nc-SiC(Szlufarska, I. et al., 2005).

A negligible degree of chemical disorder (χ = 0.008) just disorders ~3.5% of total atoms, barely affecting the topological order. Whereas these small fraction of defects prone to cluster effectively hinders the symmetrical bending of atomic layers under the indenter [Fig.

11(a)], more energy being dissipated in the atomic rearrangement of disordered clusters rather than the bending of atomic layers. As the result the onset of plastic yield occurs at much deeper depth than 3C-SiC. The slipping of atomic layers upon the critical strain is alike arrested by these embedded disordered clusters [Fig.11(b)], evidenced by the prematurely terminated dislocation propagating a relatively shorter distance compared with ones in perfect lattice [Fig.11(c)]. Further penetration of the indenter motivates the pinned dislocation which resumes propagation again as seen in Fig. 10(d). These intermittent slipping of atomic layers accounts for a slower release of accumulated stress, corresponding to the broadened and serrated peaks in the χ = 0.008 assembly. A second breaking of atomic layers triggers a following dislocation located in (111) plane with a separation of several atomic layers below the first sliding plane [Fig.11(d)]. Afterwards the bending of atomic layers overlaps with the unfolding of the previous incomplete slip. Therefore the accumulation of stress offsets partial release of load, leading to less pronounced load drop after the first peak.

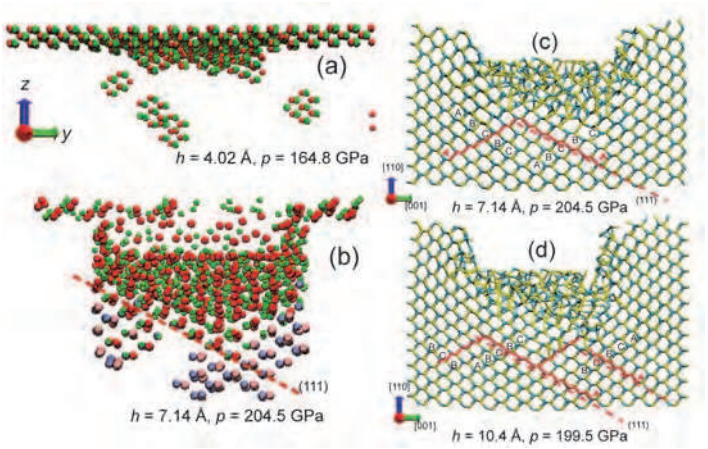

Fig. 11. The $(\bar{1}10)$ projections of indentation damages for the χ = 0.008 assembly before (a) and after (b) the first slip of atomic layers. The pink and light blue atoms refer to the chemical disordered atoms. (c) and (d) illustrate the $(\bar{1}10)$ projections of the χ = 0.008 assembly beneath the indenter after the first slip and the second slip of atomic layers, respectively.(Xue, K. & Niu, L.-S., 2010)

With increased chemical disorder (χ = 0.077), extended disordered clusters penetrating the atomic layers contribute to the substantial decay of the elastic resistance of the network. The atomic rearrangement confined in these softened regions emerges as a major energy dissipation mode complementary to the bending and slipping of atomic layers. The release of stress through localized plastic flow accounts for the remarkable reduction of hardness for the χ = 0.077 assembly. Moreover, as the continuous atomic layers are dissolved into discrete but coupled fragments cemented by disordered clusters, the discrete motions of atomic layer fragments become prevalent, which are correlated but inconsistent, for the topological environment varies from one fragment to another. Therefore one load drop in the *p-h* curve of the χ = 0.077 assembly envelops a number of correlated but uncooperative

slips of atomic layer fragments. Furthermore, the spacing between two load peaks is also no longer correlated with the separation of atomic layers in z directions.
Further increase of chemical disorder produces a percolating disordered zone through the network. The proportion of disordered atoms in the $\chi = 0.16$ assembly exceeds 17%. Then the *a*-SiC can be considered as a mixture of two coexisting phases: hard crystalline fragments and soft amorphous regions. Henceforth the discrete motion of a fragment are decoupled from those of the neighboring fragments, giving rise to the irregular fluctuations in the *p-h* curve for the $\chi = 0.16$ assembly. Both uncorrelated deformation of atomic layer fragments and enhanced plastic flow in amorphous regions contribute to the significant reduction of hardness in $\chi = 0.16$ assembly. Nevertheless, the localized plastic flow plays a dominant role in the $\chi = 0.22$ assembly, since there are no distinguishable peaks rather than small oscillations detected in the *p-h* curve for the $\chi = 0.22$ assembly.

6. Discussion

This chemical disorder based model make an initiative to quantify the correlation between mechanical properties and irradiation-amorphized SiC, while gaining valuable insights for understanding the variations of mechanical responses from the perspective of atomistic mechanisms. However we should be aware of the limitations in the conclusion drawn. The main assumption of this model is that chemical disorder underpins the changes of topological order and then determines the c-a transition of SiC. This assumption is justified by the investigation into the topological structures of a range of SiC with varying imposed level of chemical disorder. Whereas the current experimental observation could just support the existence of C-C and Si-Si homonuclear bonds, rather than provide the accurate degree of chemical disorder. Also it is agreed that the total amorphization is attained at critical threshold in deposited nuclear energy loss which is a function of ion energy and temperature(Benyagoub, A., 2008; Bolse, W., 1998). Whether the experimental measured threshold of deposited nuclear energy loss corresponds to the simulated chemical disorder is still an open question.
Incapable of describing the configuration of the defects also limits the ability of chemical order χ to characterize the structure of *a*-SiC, especially in the case involving moderate χ. For example, two *a*-SiC assemblies with identical chemical disorder may well feature distinct configurations of defects, say, one having dispersed isolated chemical disordered defects while the defects in another network tend to cluster. It is impossible to distinguish them only via chemical disorder χ. Actually, SiC exhibits different amorphization behavior in response to ion beam irradiation depending on the ion energy and ion mass. The irradiation with ions of medium mass (such as C, Si, etc) having energies of a few hundreds keV primarily produce interstitials, vacancies, antisite and small defect cluster(Gao, F. & Weber, W. J., 2001). The growth and coalescence of these point defects and small clusters correspond to partial or total amorphization. In contrast, heavy impinging ion (such as Au, etc) creates, within its displacement cascade, an amorphous zone surrounded by a defective crystalline region which in turn becomes amorphous after subsequent ion impacts, either directly by defect accumulation or indirectly by the growing of already existing amorphous zones. Therefore the c-a transition process for 3C-SiC undergoes different path depending on ion mass. Complementary to chemical disorder, additional parameter(s) containing the information about the defects configuration are necessary to describe the c-a transition.
Another issue concerning the chemical disorder based model is that it somehow underestimates the effects of Frenkel pair and vacancy clusters on the irradiation induced

amorphization. Although increased chemical disorder could simultaneously produce interstitials, vacancies and interstitial/vacancy clusters, the concentration of these defects is far from the level observed in the irradiation experiments. The current model only involving chemical disorder should be accordingly modified to take into consideration the concentrations of other defects while eliminating the overlapping effects arising from these two major defects.

7. Summary

Chemical disorder χ, a measure of the likelihood of forming homonuclear bonds in SiC controls the c-a transition occurring in the irradiation induced amorphization of SiC. A chemical disorder based model is proposed to describe the variations of different mechanical properties of SiC during the c-a transition as a function of microstructures. Elasticity and stiffness related mechanical properties of disordered SiC depend on the chemical disorder in distinct manners, which can be attributed to the different evolution stages of topological order with increasing chemical disorder. MD simulations reveal the atomistic mechanisms of varying *a*-SiC in response to tension and nanoindentation. A crossover of atomistic mechanism with damage accumulation is found in both cases, which is responsible for the evolution of mechanical responses when SiC varies from crystalline to fully amorphous. This crossover also manifests itself in the switch of fracture mode varying from brittle fracture to nano-ductile failure due to the coalescence of nanocavities.

8. Acknowledgment

The authors are grateful for funding from National Basic Research Program of China No. 2010CB631005 and State Key Laboratory of Explosion Science and Technology No. QNKT10-10 and No. ZDKT09-02.

9. References

Benyagoub, A. (2008). Irradiation Effects Induced in Silicon Carbide by Low and High Energy Ions. *Nuclear Instruments and Methods in Physics Research B*, Vol. 266, No., pp. 2766-71, 0168-583X

Bolse, W. (1998). Formation and Development of Disordered Networks in Si-Based Ceramics under Ion Bombardment. *Nuclear Instruments and Methods in Physics Research Section B: Beam Interactions with Materials and Atoms*, Vol. 141, No. 1-4, pp. 133-39, 0168-583X

Bolse, W. (1999). Amorphization and Recrystallization of Covalent Tetrahedral Networks. *Nuclear Instruments and Methods in Physics Research Section B: Beam Interactions with Materials and Atoms*, Vol. 148, No. 1-4, pp. 83-92, 0168-583X

Celarie, F.;Prades, S.;Bonamy, D.;Ferrero, L.;Bouchaud, E.;Guillot, C.&Marliere, C. (2003). Glass Breaks Like Metal, but at the Nanometer Scale. *Physical Review Letters*, Vol. 90, No. 7, pp. 075504,

Chen, H.-P.;Kalia, R. K.;Nakano, A.&Vashishta, P. (2007). Multimillion-Atom Nanoindentation Simulation of Crystalline Silicon Carbide: Orientation Dependence and Anisotropic Pileup. *Journal of Applied Physics*, Vol. 102, No. 6, pp. 063514,

Chen, Y.-C.;Lu, Z.;Nomura, K.-i.;Wang, W.;Kalia, R. K.;Nakano, A.&Vashishta, P. (2007). Interaction of Voids and Nanoductility in Silica Glass. *Physical Review Letters*, Vol. 99, No. 15, pp. 155506,

Devanathan, R.;Gao, F.&Weber, W. J. (2007). Atomistic Modeling of Amorphous Silicon Carbide Using a Bond-Order Potential. *Nuclear Instruments and Methods in Physics Research Section B: Beam Interactions with Materials and Atoms*, Vol. 255, No. 1, pp. 130-35, 0168-583X

Gao, F.&Weber, W. J. (2001). Computer Simulation of Disordering and Amorphization by Si and Au Recoils in 3c--Sic. *Journal of Applied Physics*, Vol. 89, No. 8, pp. 4275-81,

Gao, F.&Weber, W. J. (2004). Mechanical Properties and Elastic Constants Due to Damage Accumulation and Amorphization in Sic. *Physical Review B*, Vol. 69, No. 22, pp. 224108,

Heera, V.;Prokert, F.;Schell, N.;Seifarth, H.;Fukarek, W.;Voelskow, M.&Skorupa, W. (1997). Density and Structural Changes in Sic after Amorphization and Annealing. *Applied Physics Letters*, Vol. 70, No. 26, pp. 3531-33,

Hobbs, L. W.;Jesurum, C. E.&Berger, B. (1999). *Rigidity Theory and Applications* Kluwer/Plenum, New York

Ishimaru, M.;Bae, I.-T.;Hirotsu, Y.;Matsumura, S.&Sickafus, K. E. (2002). Structural Relaxation of Amorphous Silicon Carbide. *Physical Review Letters*, Vol. 89, No. 5, pp. 055502,

Ishimaru, M.;Bae, I.-T.;Hirata, A.;Hirotsu, Y.;Valdez, J. A.&Sickafus, K. E. (2006). Chemical Short-Range Order in Ion-Beam-Induced Amorphous Sic: Irradiation Temperature Dependence. *Nuclear Instruments and Methods in Physics Research Section B: Beam Interactions with Materials and Atoms*, Vol. 242, No. 1-2, pp. 473-75, 0168-583X

Ivashchenko, V. I.;Turchi, P. E. A.&Shevchenko, V. I. (2007). Simulations of the Mechanical Properties of Crystalline, Nanocrystalline, and Amorphous Sic and Si. *Physical Review B* Vol. 75, No. 8, pp. 085209,

Jiang, W.;Weber, W. J.;Lian, J.&Kalkhoran, N. M. (2009). Disorder Accumulation and Recovery in Gold-Ion Irradiated 3c-Sic. *Journal of Applied Physics*, Vol. 105, No. 1, pp. 013529,

Katoh, Y.;Hashimoto, N.;Kondo, S.;Snead, L. L.&Kohyama, A. (2006). Microstructural Development in Cubic Silicon Carbide During Irradiation at Elevated Temperatures. *Journal of Nuclear Materials* Vol. 351, No., pp. 228-40, 0022-3115

Katoh, Y.;Snead, L. L.;Henager Jr, C. H.;Hasegawa, A.;Kohyama, A.;Riccardi, B.&Hegeman, H. (2007). Current Status and Critical Issues for Development of Sic Composites for Fusion Applications. *Journal of Nuclear Materials*, Vol. 367-370, No. Part 1, pp. 659-71, 0022-3115

Khakani, M. A. E.&al, e. (1994). Hardness and Young's Modulus of Amorphous a-Sic Thin Films Determined by Nanoindentaion and Bulge Tests. *Journal of Materials Research*, Vol. 9, No. 1, pp. 96-103,

Liu, X. M. "Research on Plastic Behavior of Nano-Material Based on Dislocation Mechanism." Ph.D thesis, University of Tsinghua, 2008.

Malerba, L.&Perlado, J. M. (2001). Molecular Dynamics Simulation of Irradiation-Induced Amorphization of Cubic Silicon Carbide. *Journal of Nuclear Materials*, Vol. 289, No. 1-2, pp. 57-70, 0022-3115

Mo, Y.&Szlufarska, I. (2007). Simultaneous Enhancement of Toughness, Ductility, and Strength of Nanocrystalline Ceramics at High Strain-Rates. *Applied Physics Letters*, Vol. 90, No. 18, pp. 181926,

Mulliah, D.;Kenny, S. D.;McGee, E.;Smith, R.;Richter, A.&Wolf, B. (2006). Atomistic Modelling of Ploughing Friction in Silver, Iron and Silicon. *Nanotechnology*, Vol., No. 8, pp. 1807, 0957-4484

Noreyan, A.;Amar, J. G.&Marinescu, I. (2005). Molecular Dynamics Simulations of Nanoindentation of -Sic with Diamond Indenter. *Materials Science and Engineering B*, Vol. 117, No. 3, pp. 235-40, 0921-5107

Rino, J. P.;Ebbsj, I.;Branicio, P. S.;Kalia, R. K.;Nakano, A.;Shimojo, F.&Vashishta, P. (2004). Short- and Intermediate-Range Structural Correlations in Amorphous Silicon Carbide:A Molecular Dynamics Study. *Physical Review B*, Vol. 70, No. 4, pp. 045207,

Rodriuez de la Fuente, O.;Zimmerman, J. A.;Gonzalez, M. A.;de la Figuera, J.;Hamilton, J. C.;Pai, W. W.&Rojo, J. M. (2002). Dislocation Emission around Nanoindentations on a (001) Fcc Metal Surface Studied by Scanning Tunneling Microscopy and Atomistic Simulations. *Physical Review Letters*, Vol. 88, No. 3, pp. 036101,

Rong, Z.;Gao, F.;Weber, W. J.&Hobler, G. (2007). Monte Carlo Simulations of Defect Recovery within a 10 Kev Collision Cascade in 3c--Sic. *Journal of Applied Physics*, Vol. 102, No. 10, pp. 103508,

Shi, Y.&Falk, M. L. (2005). Strain Localization and Percolation of Stable Structure in Amorphous Solids. *Physical Review Letters*, Vol. 95, No. 9, pp. 095502,

Snead, L. L.;Steiner, D.&Zinkle, S. J. (1992). Measurement of the Effect of Radiation Damage to Ceramic Composite Interfacial Strength. *Journal of Nuclear Materials*, Vol. 191-194, No. Part 1, pp. 566-70, 0022-3115

Snead, L. L.;Zinkle, S. J.;Hay, J. C.&Osborne, M. C. (1998). Amorphization of Sic under Ion and Neutron Irradiation. *Nuclear Instruments and Methods in Physics Research Section B: Beam Interactions with Materials and Atoms*, Vol. 141, No. 1-4, pp. 123-32, 0168-583X

Snead, L. L.&Zinkle, S. J. (2002). Structural Relaxation in Amorphous Silicon Carbide. *Nuclear Instruments and Methods in Physics Research Section B: Beam Interactions with Materials and Atoms*, Vol. 191, No. 1-4, pp. 497-503, 0168-583X

Snead, L. L. (2004). Limits on Irradiation-Induced Thermal Conductivity and Electrical Resistivity in Silicon Carbide Materials. *Journal of Nuclear Materials*, Vol. 329-333, No., pp. 524-29, 0022-3115

Snead, L. L.;Nozawa, T.;Katoh, Y.;Byun, T.-S.;Kondo, S.&Petti, D. A. (2007). Handbook of Sic Properties for Fuel Performance Modeling. *Journal of Nuclear Materials*, Vol. 371, No., pp. 329-77, 0022-3115

Szlufarska, I.;Kalia, R. K.;Nakano, A.&Vashishta, P. (2004). Nanoindentation-Induced Amorphization in Silicon Carbide. *Applied Physics Letters*, Vol. 85, No. 3, pp. 378-80,

Szlufarska, I.;Kalia, R. K.;Nakano, A.&Vashishta, P. (2005). Atomistic Mechanisms of Amorphization During Nanoindentation of Sic: A Molecular Dynamics Study. *Physical Review B*, Vol. 71, No. 17, pp. 174113,

Szlufarska, I.;Nakano, A.&Vashishta, P. (2005). A Crossover in the Mechanical Response of Nanocrystalline Ceramics. *Science*, Vol. 309, No. 5736, pp. 911-14,

Szlufarska, I.;Kalia, R. K.;Nakano, A.&Vashishta, P. (2007). A Molecular Dynamics Study of Nanoindentation of Amorphous Silicon Carbide. *Journal of Applied Physics*, Vol. 102, No. 2, pp. 023509,

Tang, M.&Yip, S. (1995). Atomistic Simulation of Thermomechanical Properties of Beta -Sic. *Physical Review B*, Vol. 52, No. 21, pp. 15150,

Tersoff, J. (1994). Chemical Order in Amorphous Silicon Carbide. *Physical Review B*, Vol. 49, No. 23, pp. 16349,

Weber, W. J.;Yu, N.;Wang, L. M.&Hess, N. J. (1997). Temperature and Dose Dependence of Ion-Beam-Induced Amorphization in [Alpha]-Sic. *Journal Of Nuclear Materials*, Vol. 244, No. 3, pp. 258-65, 0022-3115

Weber, W. J.;Wang, L. M.;Yu, N.&Hess, N. J. (1998). Structure and Properties of Ion-Beam-Modified (6h) Silicon Carbide. *Materials Science and Engineering A*, Vol. 253, No. 1-2, pp. 62-70, 0921-5093

Xi, X. K.;Zhao, D. Q.;Pan, M. X.;Wang, W. H.;Wu, Y.&Lewandowski, J. J. (2005). Fracture of Brittle Metallic Glasses: Brittleness or Plasticity. *Physical Review Letters*, Vol. 94, No. 12, pp. 125510,

Xue, K.;Niu, L.-S.&Shi, H.-J. (2008). Effects of Quench Rates on the Short- and Medium-Range Orders of Amorphous Silicon Carbide: A Molecular-Dynamics Study. *Journal of Applied Physics*, Vol. 104, No. 5, pp. 053518,

Xue, K.&Niu, L.-S. (2009). Understanding the Changes in Mechanical Properties Due to the Crystalline-to-Amorphization Transition in Sic. *Journal of Applied Physics*, Vol. 106, No. 6, pp. 083505,

Xue, K.&Niu, L.-S. (2010). A Crossover in the Mechanical Response of Silicon Carbide Due to the Accumulation of Chemical Disorder. *Journal of Applied Physics*, Vol. 107, No. 8, pp. 083517,

Yuan, X.&Hobbs, L. W. (2002). Modeling Chemical and Topological Disorder in Irradiation-Amorphized Silicon Carbide. *Nuclear Instruments and Methods in Physics Research Section B: Beam Interactions with Materials and Atoms*, Vol. 191, No. 1-4, pp. 74-82, 0168-583X

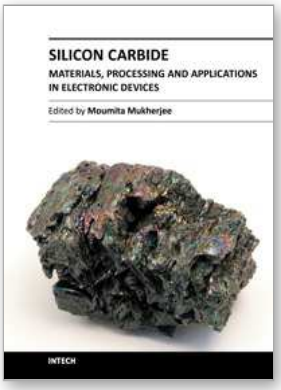

Silicon Carbide - Materials, Processing and Applications in Electronic Devices

Edited by Dr. Moumita Mukherjee

ISBN 978-953-307-968-4
Hard cover, 546 pages
Publisher InTech
Published online 10, October, 2011
Published in print edition October, 2011

Silicon Carbide (SiC) and its polytypes, used primarily for grinding and high temperature ceramics, have been a part of human civilization for a long time. The inherent ability of SiC devices to operate with higher efficiency and lower environmental footprint than silicon-based devices at high temperatures and under high voltages pushes SiC on the verge of becoming the material of choice for high power electronics and optoelectronics. What is more important, SiC is emerging to become a template for graphene fabrication, and a material for the next generation of sub-32nm semiconductor devices. It is thus increasingly clear that SiC electronic systems will dominate the new energy and transport technologies of the 21st century. In 21 chapters of the book, special emphasis has been placed on the â€œmaterialsâ€ aspects and developments thereof. To that end, about 70% of the book addresses the theory, crystal growth, defects, surface and interface properties, characterization, and processing issues pertaining to SiC. The remaining 30% of the book covers the electronic device aspects of this material. Overall, this book will be valuable as a reference for SiC researchers for a few years to come. This book prestigiously covers our current understanding of SiC as a semiconductor material in electronics. The primary target for the book includes students, researchers, material and chemical engineers, semiconductor manufacturers and professionals who are interested in silicon carbide and its continuing progression.

How to reference

In order to correctly reference this scholarly work, feel free to copy and paste the following:

Kun Xue, Li-Sha Niu and Hui-Ji Shi (2011). Mechanical Properties of Amorphous Silicon Carbide, Silicon Carbide - Materials, Processing and Applications in Electronic Devices, Dr. Moumita Mukherjee (Ed.), ISBN: 978-953-307-968-4, InTech, Available from: http://www.intechopen.com/books/silicon-carbide-materials-processing-and-applications-in-electronic-devices/mechanical-properties-of-amorphous-silicon-carbide

INTECH
open science | open minds

InTech Europe
University Campus STeP Ri
Slavka Krautzeka 83/A
51000 Rijeka, Croatia
Phone: +385 (51) 770 447
Fax: +385 (51) 686 166

InTech China
Unit 405, Office Block, Hotel Equatorial Shanghai
No.65, Yan An Road (West), Shanghai, 200040, China
中国上海市延安西路65号上海国际贵都大饭店办公楼405单元
Phone: +86-21-62489820
Fax: +86-21-62489821